Calculation of the Conformation Entropies of Dimer Liquid Crystals and Comparison with the Observed Transition Entropies at Constant Volume

Akihiro Abe,* Hidemine Furuya, Renato N. Shimizu, and Su Yong Nam

Department of Polymer Chemistry, Tokyo Institute of Technology, Ookayama, Meguro-ku, Tokyo 152, Japan

Received April 11, 1994; Revised Manuscript Received October 5, 1994[⊗]

ABSTRACT: RIS analysis of the deuterium quadrupolar splitting data was performed for α,ω-bis[(4,4′-cyanobiphenylyl)oxy]alkane dimer liquid crystals having $-O(CH_2)_nO-$ flexible spacers (n = 9 (CBA-9) and n = 10 (CBA-10)) between the 4,4′-cyanobiphenylyl ends according to the scheme previously established. The analysis indicates that most of the conformers involved in the range $0 < \psi_1,\psi_2 < 45°$ adopt spatial configurations reasonably consistent with the nematic arrangement of mesogenic cores in both dimer LC systems, where ψ_1 and ψ_2 denote the inclination angles of the terminal mesogenic cores with respect to the molecular axis. The conformational entropy changes at the crystal−nematic (CN) and nematic−isotropic (NI) interphases estimated on this basis are as follows: CBA-9, ΔS_{cn}^{conf} = 59.6, ΔS_{ni}^{conf} = 13.3; CBA-10, ΔS_{cn}^{conf} = 64.2, ΔS_{ni}^{conf} = 15.6 (J mol^{-1} K^{-1} units). The values of the entropies ΔS_{tr}^{conf} thus derived were compared with the constant-volume transition entropies $(\Delta S_{tr})_v$ determined by the *PVT* measurements reported in the accompanying paper: CBA-9, $(\Delta S_{cn})_v$ = 53.9, $(\Delta S_{ni})_v$ = 7.9; CBA-10, $(\Delta S_{cn})_v$ = 62.4, $(\Delta S_{ni})_v$ = 13.3 (J mol^{-1} K^{-1} units). In view of the uncertainties involved in the estimation of the entropies both in theory and in experiments, the correspondence is quite favorable. The conformation of the spacer undoubtedly plays an important role in determining the phase behaviors of these main chain liquid crystals. It is pointed out that the discrepancy between the calculation and experiment may be further improved by considering other contributions such as (1) the entropy changes due to the orientation of the anisotropic molecules in the liquid crystalline state and (2) the possibility of the entropy loss during the compression to achieve constant-volume transitions. It is concluded that the observed increase in the quadrupolar and dipolar splittings with decreasing temperature arises mainly from the variation of the order parameter of the molecular axis.

1. Introduction

The order−disorder transition of liquid crystals normally proceeds stepwise from the crystalline state to the isotropic melt. Dimer liquid crystals (DLCs) such as

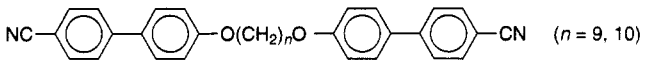

exhibit sharp crystal ↔ nematic (CN) and nematic ↔ isotropic (NI) transitions. In the preceding paper[1] (hereafter referred to as Paper 1), we have reported the results of pressure−volume−temperature (*PVT*) measurements on these systems. The transition entropies at constant volume, denoted as $(\Delta S_{cn})_v$ and $(\Delta S_{ni})_v$ respectively for the above-mentioned transitions, have been determined using the thermodynamic relation

$$(\Delta S_{tr})_v = \Delta S_{tr} - (\alpha/\beta)\Delta V_{tr} \qquad (1)$$

where ΔS_{tr} denotes the transition entropy observed under constant pressure, α is the thermal expansion coefficient, β is the isothermal compressibility, and ΔV_{tr} is the volume change at the transition. The constant-volume entropies estimated in this manner include two major contributions: (1) variation in the orientational distribution of anisotropic mesogenic units and (2) conformational change of the flexible spacer. The relative importance of these factors may be inspected from previous *PVT* studies on low-molar-mass liquid crystals (MLC) with relevant chemical structures[2,3] as well as from similar analyses on conventional chain molecules.[4]

MLCs are often composed of a rigid mesogenic core and flexible tail(s). Flexible tails are known to play an important role in stabilizing the liquid crystalline phase. According to the literature, the transition entropy ΔS_{ni} usually decreases as the flexible tail becomes shorter, suggesting that some appreciable contribution arises from the conformation of the appended tail.[2,5]

In treating melting behaviors of chain molecules, the constant-volume entropy obtained as above is often identified with the contribution arising from the variation in the spatial configuration of chains on going from the crystalline to the molten amorphous state, ΔS^{conf}.[6,7] For long chain molecules, the contribution from the communal entropy is assumed to be relatively small.[4,8] In fact, values of $(\Delta S_{tr})_v$ experimentally derived are usually in good agreement with those ΔS^{conf} theoretically calculated.[6,7] In spite of its popularity, however, the validity of the assumption is sometimes questioned by saying that the agreement may be due to a fortuitous cancellation of errors. The major criticism arises from the possibility that the conformational entropy may decrease by the compression required to achieve the constant-volume disorder.[9−12] From Table 6 of Paper 1, the sum of the two transition entropies $(\Delta S_{cn})_v + (\Delta S_{ni})_v$ amounts to 61.8 and 75.7 J mol^{-1} K^{-1}, respectively, for CBA-9 and -10. Attributing these entropies to the flexible methylene units in the spacer, we obtain 6.9 and 7.6 J K^{-1} (mol of CH_2)$^{-1}$. The corresponding value in a long polymethylene chain is known to be in a similar range 7−9 J K^{-1} (mol of CH_2)$^{-1}$. Would it be a mere coincidence? Or would it suggest that the phase transition entropies $(\Delta S_{tr})_v$ of DLCs are mostly conformational? This is the subject of the present paper.

[⊗] Abstract published in *Advance ACS Abstracts,* December 1, 1994.

0024-9297/95/2228-0096$09.00/0

In a 1984 paper,[13] Abe discussed the conformational characteristics of the polymethylene sequence comprising a series of tetrahedral sp^3 bonds. The results of the analysis on ester and ether type main chain LCs indicate that the distribution of the angle θ defined by the two terminal mesogenic core axis is essentially bimodal in the unconstrained free state: with the spacer comprising an odd number (n) of carbons, $\theta = 50-90°$ and $160-180°$ and with that of n = even, $\theta = 0-30°$ and $85-130°$. It has been concluded that the high-angle mode should be suppressed when these molecules adopt the nematic order. Later, Abe and Furuya[14] proposed a RIS model to elucidate the conformation of the spacer involved in the main chain dimer and polymer LCs on the basis of ^{2}H NMR quadrupolar splitting data. This model has been derived[15] on the assumptions that (1) the molecular axis (Z) lies in the direction parallel to the line connecting the center of two neighboring mesogenic cores and (2) the molecules are approximately axially symmetric around the Z-axis, and thus the orientation of anisotropic molecules can be described by a single order parameter S_{ZZ}. These assumptions enable us to extract the conformational contribution from the observed order parameter which represents the orientation of the overall molecule in the nematic environment. DLCs, PLCs, and copolymers in which spacers n = 9 and 10 are arranged in an alternate fashion were examined in this scheme.[16,17] The ordering characteristics thus estimated were found to be consistent with the magnetic susceptibility data obtained by using the superconducting quantum interference device (SQUID) for the same DLCs and PLCs.[18] More recently, conformational characteristics of the spacer were examined in binary mixtures comprising dimer and monomer LCs. An important consequence of this work is that the nematic conformation of the spacer remains quite stable over a wide range of concentration and varies only slightly with temperature.[19,20] In the present study, we have investigated the stability of the nematic conformation in the bulk state. The conformational analysis has been performed carefully to achieve an accurate estimate of the nematic fraction, based on which the conformational entropy changes at the CN and NI transitions may be calculated. Comparison of the results with those reported in Paper 1 should provide some insight regarding the phase transition mechanism of the main chain type LCs.

2. Samples and Measurements

The preparation of α,ω-bis[(4,4′-cyanobiphenylyl)oxy]alkane (CBA-n) has been reported elsewhere.[21] The samples carrying perdeuterated spacers were obtained by starting from perdeuterated α,ω-dibromoalkanes, $Br(CD_2)_nBr$ with n = 9 and 10. Substitution of deuterons at the ortho position of the 4,4′-cyanobiphenyl group was easily accomplished by the standard method.[19]

The ^{2}H NMR spectra were recorded on a JEOL JNM-GSX-500 spectrometer operating at a 76.65 MHz deuterium resonance frequency. Measurements were carried out under a complete decoupling and nonspinning mode. In the experiment, samples initially kept at a temperature above T_{ni} were cooled slowly to get into the nematic mesophase. Since observations were performed in the cooling mode, the nematic phase persisted over a wide temperature range due to an appreciable supercooling effect: 172−110 °C for CBA-9 and 185−135 °C for CBA-10. The assignment of the individual splittings to the methylene groups of the spacer has been worked out previously by using partially deuterated DLC samples.[21]

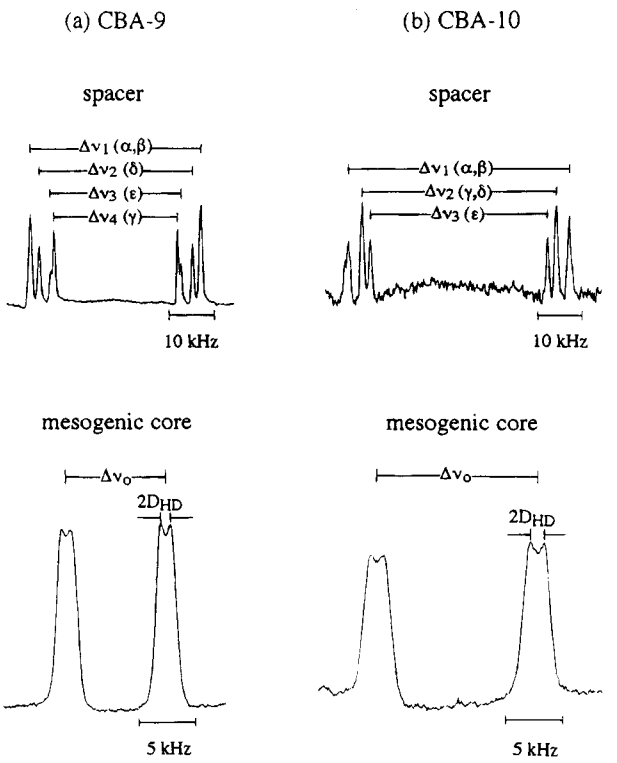

Figure 1. Examples of ^{2}H NMR spectra observed in the vicinity of T_{ni}: (a) CBA-9; (b) CBA-10. The assignments of $\Delta\nu_i$ to the individual methylene groups are indicated in parentheses.

Table 1. Values of $\Delta\nu_0$ and D_{HD} Observed for the Mesogenic Core Deuterated at the Ortho Position

temp (°C)	$\Delta\nu_0$ (kHz)	D_{HD} (kHz)	temp (°C)	$\Delta\nu_0$ (kHz)	D_{HD} (kHz)
		CBA-9			
173.4	7.3	0.33	165.1	10.5	0.50
172.8	7.4	0.31	160.0	11.7	0.54
172.4	7.9	0.34	155.0	12.4	0.56
171.8	8.2	0.37	150.1	12.9	0.59
171.0	8.6	0.42	135.0	14.6	0.61
170.1	9.0	0.45			
		CBA-10			
184.0	12.6	0.54	175.0	15.5	0.61
183.5	12.8	0.46	170.0	16.5	0.64
183.0	12.9	0.56	165.0	17.4	0.58
182.0	13.3	0.48	160.0	18.0	0.62
181.0	13.8	0.55	150.1	19.1	0.65
180.0	14.1	0.59			

3. Results of ^{2}H NMR Measurements

Examples of ^{2}H NMR spectra for the deuterated mesogenic core and spacer are shown in Figure 1 for CBA-9 and -10. The doublet $\Delta\nu_0$ due to dipolar splittings (D_{HD}) originates from the C−D bond at the ortho position of the mesogenic core. Assignments of the observed quadrupolar splittings $\Delta\nu_i$ to the individual spacer methylene units are indicated in the diagram. The observed values of $\Delta\nu_0$ and D_{HD} are summarized in Table 1. The quadrupolar splittings $\Delta\nu_i$ for the spacer were determined separately, and the results are given in Table 2. The order parameters of the mesogenic core axis S^R_{ZZ} and $S^R_{XX} - S^R_{YY}$ can be easily estimated from the observed D_{HD} in combinatiuon with $\Delta\nu_0$ according to the scheme previously described.[22] Variations of these order parameters as a function of temperature are indicated in Figure 2: the contribution from the biaxiality term $S^R_{XX} - S^R_{YY}$ remains small, the magnitude being of the order of 0−0.04 over the temperature range

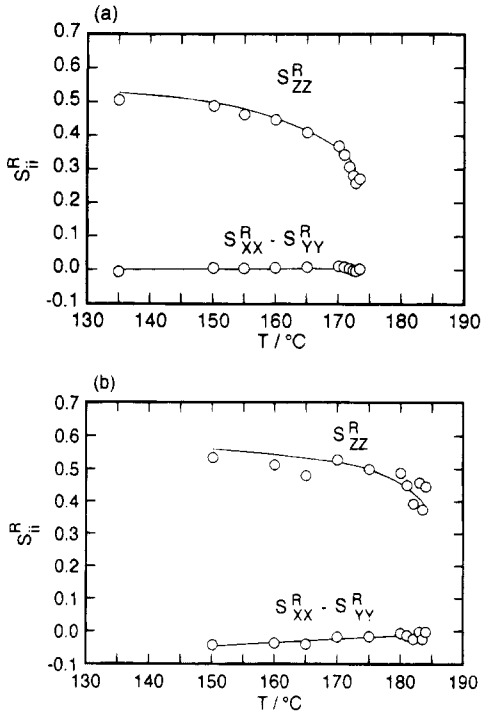

Figure 2. Variation of the order parameters of the mesogenic core as a function of temperature: (a) CBA-9; (b) CBA-10.

Table 2. Observed Values of $\Delta\nu_i$ for the Spacer, the Assignments of the Individual Splittings Being Given in Figure 1

temp (°C)	$\Delta\nu_1$ (kHz)	$\Delta\nu_2$ (kHz)	$\Delta\nu_3$ (kHz)	$\Delta\nu_4$ (kHz)
		CBA-9		
172.8	33.6	29.9	25.0	24.3
171.8	33.9	30.3	25.1	24.2
169.8	38.1	34.3	29.1	27.6
165.0	43.6	39.8	33.9	32.1
154.8	50.0	46.5	40.0	37.7
140.0	56.3	54.0	46.9	44.1
130.0	59.9	58.3	51.0	47.8
		CBA-10		
184.8	46.3	40.9	37.2	
183.5	48.4	42.6	38.9	
181.5	50.7	45.0	41.3	
175.8	55.1	49.8	45.7	
164.9	61.1	56.6	52.1	
155.0	65.4	61.6	56.8	
145.0	69.1	65.6	60.9	

studied. Following our previous analysis,[19] the ratios $\Delta\nu_i/\Delta\nu_1$ ($i > 1$) defined for the spacer are plotted against T in Figure 3, for the CBA-9 and -10. As will be mentioned in due course, the temperature dependence of such ratios mainly arises from the variation of the spacer conformation.

4. RIS Analysis

4.1. Simulation of ^{2}H NMR Profiles. Bond lengths and bond angles required for the RIS description of the flexible spacer were taken from our previous publication.[14] For simplicity, the mesogenic cores are treated as a simple rod with a center at a distance of 5 Å from the oxygen atom, the value roughly corresponding to the chemical structure. The skeletal carbons of the spacer are numbered from 1 to 5 (for $n = 9$) and from 1 to 6 (for $n = 10$) from one terminal to the midchain. Because of the symmetry of the molecules, distinction beyond the middle is redundant. The O–C_1 and the C_{i-1}–C_i bonds are numbered as 1 and i, respectively. Statistical weight factor σ_i was assigned to the gauche state of the

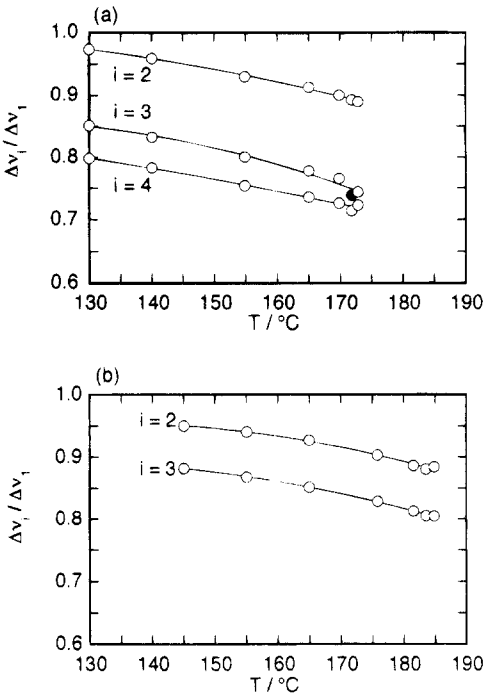

Figure 3. Quadrupolar splitting ratios $\Delta\nu_i/\Delta\nu_1$ observed for the spacer plotted against temperature: (a) CBA-9; (b) CBA-10.

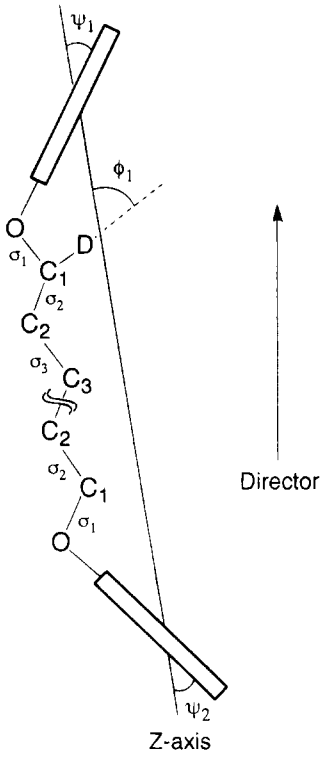

Figure 4. Definition of the molecular axis and the statistical weights σ_i assigned to the gauche state of the ith bond. ψ_1 and ψ_2 are the inclinations of the mesogenic cores, and ψ_i represents the angle between the ith C–D bond and the molecular axis.

ith C–C bond, the weight of unity being given to the corresponding trans state (cf. Figure 4).

The RIS calculations were first performed for molecules in the unconstrained isotropic state, thereby all possible conformations of the spacer $-O(CH_2)_nO-$ being elucidated. For each given spatial arrangement of molecules, the molecular axis was defined as illustrated in Figure 4, and the inclination angles of the terminal

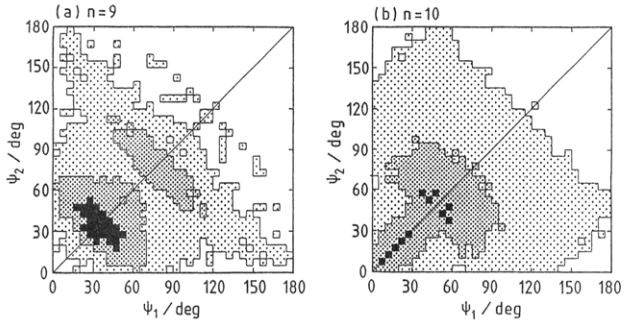

Figure 5. Conformational distribution map (ψ_1, ψ_2) calculated for the temperature of 500 K: (a) CBA-9; (b) CBA-10. The population densities of the conformation (per 5° × 5° square) are distinguished into three ranks: filled (>1.0%), heavily dotted (0.1−1.0%), and lightly dotted (<0.1%).

mesogenic cores ψ_1 and ψ_2 were calculated. Conventional values of the conformational energy parameter were adopted in the calculation of population densities: $E_{\sigma_1} = 5.9$, $E_{\sigma_2} = 0$, $E_{\sigma_i} = 2.1$ with $i = 3-5$ (for $n = 9$) and $i = 3-6$ (for $n = 10$), $E_\omega = 8.4$ for the second-order interaction involved in CC−C−CC, and $E_{\omega'} = 2.1$ for OC−C−CC, all energies being in kJ mol^{-1}. The temperature was set equal to 500 K. The distributions of the conformations (ψ_1, ψ_2) are indicated on the map in Figure 5, where the population densities of the conformation (per 5° × 5° square) are distinguished into three ranks: filled (>1%), heavily dotted (0.1−1.0%), and lightly dotted (<0.1%). The conformation maps shown in Figure 5 are essentially identical to those previously reported:[14] the diagrams are symmetric around $\psi_1 = \psi_2$, and the distributions are bimodal.[13] The distinction between the two figures represents the odd−even character of the polymethylene sp^3 bonding system.

Under a nematic constraint, distribution of the conformer should be restricted within a certain range of the (ψ_1, ψ_2) map. The second-order interactions $g^{\pm}g^{\mp}$ were assumed to be essentially suppressed. Following previous treatment,[14] conformations having ψ's larger than a certain critical value ψ_m were excluded from the nematic fraction. Hereafter, we designate this fraction as F-ψ_m. For an ensemble of spatial configurations thus selected, the simulation of ^{2}H NMR spectra was attempted as described below. In practice, ψ_m was treated as an adjustable parameter in the iterative calculation.

With the molecular axis as defined in Figure 4, the following expressions may be adopted for the dipolar coupling D_{HD} due to the mesogenic units and the quadrupolar splitting $\Delta\nu_i$ of the ith C−D bond of the spacer:

$$D_{HD} = -[\gamma_H\gamma_D h/(4\pi^2 r_{HD}{}^3)]S_{ZZ}(3\langle\cos^2\psi\rangle - 1)/2 \quad (2)$$

$$\Delta\nu_i = (3/2)(e^2qQ/h)S_{ZZ}(3\langle\cos^2\phi_i\rangle - 1)/2 \quad (3)$$

where the coupling constants were taken to be $\gamma_H\gamma_D h/(4\pi^2 r_{HD}{}^3) = 1.209$ kHz and $(e^2qQ/h) = 174$ kHz. The angle ϕ_i represents the inclination of the ith C−D bond with respect to the molecular axis Z (cf. Figure 4), and the angular brackets denote the statistical mechanical average over all allowed conformations. Here we assume that the molecules are approximately axially symmetric around the Z-axis, and the orientation of such anisotropic molecules can be described by a single order parameter S_{ZZ}, the biaxiality of the system $S_{XX} - X_{YY}$ being ignored for simplicity. Within this approximation, the molecular order parameter S_{ZZ} can be eliminated by taking ratios of these expressions:

$$D_{HD}/\Delta\nu_j = -C(3\langle\cos^2\psi\rangle - 1)/(3\langle\cos^2\phi_j\rangle - 1) \quad (4)$$

$$\Delta\nu_i/\Delta\nu_j = (3\langle\cos^2\phi_i\rangle - 1)/(3\langle\cos^2\phi_j\rangle - 1) \qquad (i \neq j) \quad (5)$$

where $C = [\gamma_H\gamma_D h/(4\pi^2 r_{HD}{}^3)]/(3e^2qQ/2h)$ is a constant. Since parameters ϕ and ψ are the angles defined in the internal coordinate system, these ratios can be directly related to the conformation of the spacer. The averages $\langle\cos^2\phi_i\rangle$ and $\langle\cos^2\psi\rangle$, respectively, for the ith C−D bond of the spacer and the mesogenic core axis may be estimated for any given conformer distribution. Use of eqs 4 and 5 may yield $\Delta\nu_i$ with either a positive or negative sign. Comparison with experimental observations requires only absolute values of $\Delta\nu_i$. Experimental values of the ratio $\Delta\nu_i/\Delta\nu_j$ vary somewhat (several percent) as a function of temperature, implying that the conformation of the spacer may be affected similarly: e.g., d $\ln(\Delta\nu_i/\Delta\nu_1)/dT$ = ca. -2×10^{-3} K^{-1} (see Figure 3).

In our previous papers, attempts have been made to elucidate conformation from ^{2}H NMR spectra by assuming a simple relation such as

$$\langle\cos^2\phi\rangle = \sum_k[\cos^2\phi(\prod_{i=1}^{n-1}s_i)]_k/\sum_k(\prod_{i=1}^{n-1}s_i)_k \quad (6)$$

where s_i represents the weight for bond i, i.e., 1 or σ_i, in the kth configuration. In the iterative calculations, the simplex method was extensively employed to monitor the convergence of the iteration by minimizing the reliability factor,

$$R\ (\%) = \left[\frac{\sum(A_{calcd} - A_{obsd})^2}{\sum A_{obsd}{}^2}\right]^{1/2} \times 100 \quad (7)$$

In this work, we have carried out simulations by starting from various initial combinations of σ_i's defined in the range 0−1. Convergencies of the iteration were attained for the conformer set defined by $\psi_m = 40-45°$ for CBA-9 and 35−45° for CBA-10 on the conformation map (cf. Figure 5). The results of simulations with $\psi_m = 45°$ are illustrated by the solid lines in Figure 6, where the corresponding experimental $\Delta\nu$ values are indicated by circles. Comparisons are illustrated for two temperatures: one in the vicinity of T_{ni} and the other around the observed melting temperature T_m. The agreement is nearly perfect in all examples. Spatial arrangements of the spacer should tend to be random as much as possible in the liquid-crystalline state provided that they are compatible with the nematic environment. We thus adopt the conformer ensemble corresponding to higher ψ_m values. In the latter sections, the ensemble corresponding to $\psi_m = 45°$ (i.e., F-45) will be extensively examined.

For the purpose of elucidating the conformational entropies of the nematic state, an account of the contribution from all allowed conformer species is a prerequisite. Since the relation given in eq 6 is incapable of taking account of the long-range correlation of bond conformations along the chain, the efficiency of the technique may be limited. Such long-range correlations are especially marked in the CBA-10 system. As easily shown by a molecular model, the conformational cor-

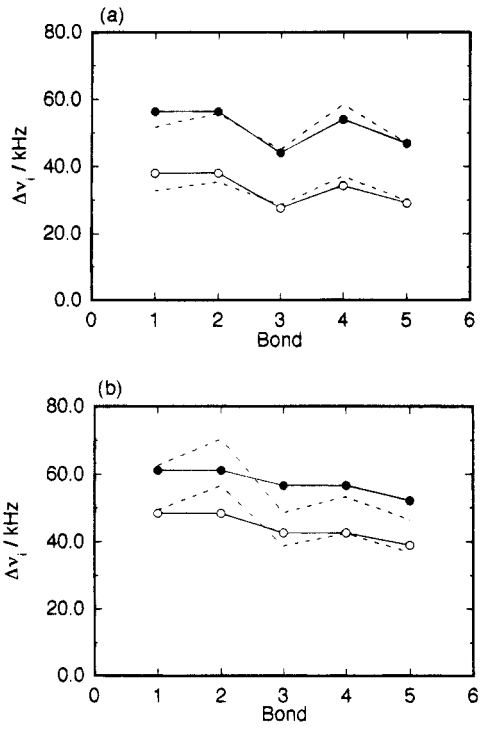

Figure 6. Quadrupolar splittings $\Delta\nu_i$ plotted against carbon number i. Shown by open and filled circles are the experimental values observed in the vicinity of T_{ni} and T_m, respectively: (a) CBA-9, (○) 169.8 °C, (●) 140.0 °C; (b) CBA-10, (○) 183.5 °C, (●) 164.9 °C. Solid lines indicate the best-fit results obtained by using the RIS simulation for F-45. Dashed lines are those calculated directly from F-45 (without simulation).

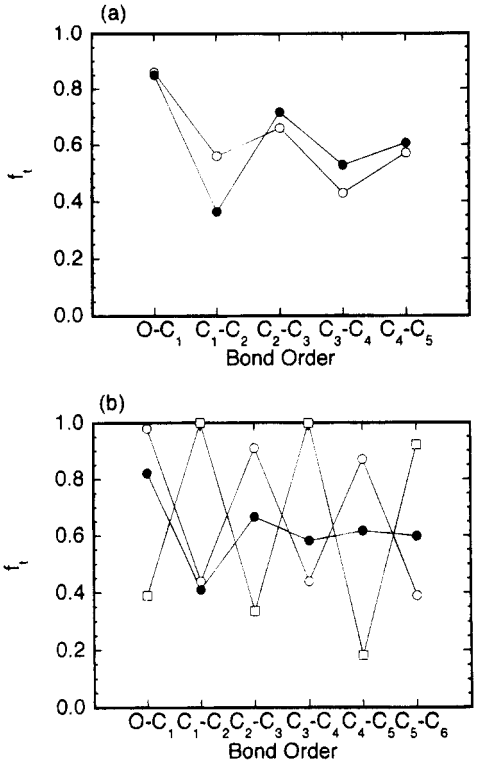

Figure 7. Bond conformation of the internal O−C and C−C bonds in the nematic phase. The fractions of the trans conformer (f_t) are shown in the order from the terminal to the central bond. (a) CBA-9: calculated on the basis of F-45 with (○) and without (●) RIS simulation. (b) CBA-10: open circles and squares indicate two representative odd−even trends found in the RIS simulation of F-45, both being consistent with the results of ^{2}H NMR (see text). Filled circles are those directly calculated from F-45 (without simulation).

relation along the chain is less distinct when the spacer comprises an odd number of carbon atoms.

4.2. Determination of the Nematic Conformation. In order not to exclude any minor fractions which may exist in the nematic state, conformers involved in F-45 were carefully examined according to their conformational correlation patterns along the spacer. The results are briefly summarized below:

(1) CBA-9. A satisfactory reproduction of experimental data was confirmed by the simulation on the conformer ensemble F-45. The bond conformations obtained are somewhat divergent depending on the initial parameter set. The values of $\Delta\nu$, D_{HD}, and bond conformations were also calculated directly (without simulation) from the ensemble F-45, the agreement being optimized by minimizing the R value. The results obtained at two temperatures are compared with those derived from the RIS simulation in Figure 6a. The agreements in $\Delta\nu$ are somewhat less satisfactory in the former calculation. The bond conformation vs bond order plots derived concomitantly are shown in Figure 7a. The results obtained with and without simulation resemble each other except for the C_1−C_2 bond. The values of D_{HD} calculated are found to be consistent with those observed: obsd/calcd, 0.45 (±0.10)/0.38 (169.8 °C) and 0.60 (±0.10)/0.61 (140.0 °C) (kHz units). These results indicate that the conformers involved in the ensemble F-45 are mostly compatible with the nematic environment. It should also be noted that the conformational partition function was found to remain nearly identical before and after the simulation.

(2) CBA-10. In this work, we have found that the RIS simulation of CBA-10 for the ensemble F-45 converges into either of the two conformer distributions depending on the initial parameter set. These two groups can be distinguished from each other by the odd−even character of the bond conformation along the chain: e.g., tgt vs gtg for a given triad. The results of the RIS simulation mostly fall into the "odd−even" group reported in the previous papers. Although the sequences having an opposite odd−even character occur less frequently in the simulation, their contribution to the transition entropy may not be negligible. Under these circumstances, we must admit that the simulation scheme set forth above is not competent to elucidate the whole nematic conformer of CBA-10. Following the treatment described above for CBA-9, we have examined the conformational characteristics of F-45 by calculating $\Delta\nu$, D_{HD}, and bond conformations for two different temperatures. For CBA-10, the agreements in $\Delta\nu$ are only moderate (Figure 6b). As mentioned above, the experimental ^{2}H NMR profiles can be reproduced by either of the two conformer groups derived from the RIS simulation of F-45 (see solid lines in Figure 6b). The odd−even oscillations of the bond conformation characteristic to these two groups are indicated by open circles and squares in Figure 7b. The oscillation becomes less pronounced for the conformations calculated from the original F-45 (i.e., without simulation) (filled circles). In contrast to the CBA-9 system, the values of D_{HD} tend to be overestimated when calculated directly from F-45: obsd/calcd, 0.46 (±0.10)/0.73 (183.5 °C) and 0.58 (±0.10)/0.94 (164.9 °C) (kHz units). In the present study, an extensive conformer analysis was carried out for F-45 to understand the conformational characteristics of the ensemble. Each of the three major conformational correlation patterns exhibits different

Table 3. Comparison of Calculated Conformational Entropy with Constant-Volume Transition Entropy Derived from *PVT* Measurements

CN transition			NI transition		
temp (°C)	ΔS_{cn}^{conf} (J mol^{-1} K^{-1})	$(\Delta S_{cn})_v$[a] (J mol^{-1} K^{-1})	temp (°C)	ΔS_{ni}^{conf} (J mol^{-1} K^{-1})	$(\Delta S_{ni})_v$[a] (J mol^{-1} K^{-1})
		CBA-9			
140.0	59.6	53.9	169.8	13.3	7.9
		CBA-10			
164.9	64.2	62.4	183.5	15.6	13.3

[a] Taken from Table 6 of Paper 1.

contributions to the $\Delta\nu$ and D_{HD} values. The details are described in the Appendix.

Since the bond conformations estimated at two different temperatures are nearly identical in both CBA-9 and CBA-10, those obtained at lower temperatures are not shown in Figure 7. These results suggest that the observed increase in D_{HD} and $\Delta\nu$ with decreasing temperature (cf. Tables 1 and 2) arises mainly from the variation of the order parameter of the molecular axis S_{ZZ}, the conformation of the spacer remaining quite stable in the nematic phase. In the following, the entropy changes at the CN and NI interphases will be estimated on the basis of the nematic conformation F-45.

4.3. Estimation of Conformational Entropy. With the nematic conformation thus defined, the transition entropies at the CN and NI interphase may be estimated. Malpezzi et al.[23] reported the results of the X-ray analysis on a CBA-7 single crystal, concluding that the spacer, $-O(CH_2)_7O-$, was in the all-trans conformation. We may assume that CBA-9 and -10 also exist in a similar conformation in the solid state. In the isotropic melt, they should take a random-coil arrangement.[24] The difference in the conformational entropy between the two states can be calculated on the basis of the conformational partition function of the individual states. I.e., for the NI transition,

$$\Delta S_{ni}^{conf} = -R \ln(z_n/z_i) + (\langle E\rangle_i - \langle E\rangle_n)/T_{ni} \qquad (8)$$

where z and $\langle E\rangle$ denote, respectively, the partition function and average energy of the state as specified by the subscript. In these calculations, the all-trans conformation was taken to be the reference state: thus $z_c = 1$ and $E_c = 0$. Values of z_n and $\langle E\rangle_n$ can be estimated from the nematic fraction F-45 in the vicinity of T_{ni}. The corresponding quantities for the isotropic state, z_i and $\langle E\rangle_i$, may be obtained by the conventional RIS treatment of the molecular system. The transition entropies, ΔS_{ni}^{conf}, calculated in this manner are given in Table 3.

The conformational entropy change for the CN transition may be estimated by using a similar expression:

$$\Delta S_{cn}^{conf} = R \ln z_n + \langle E\rangle_n/T_{cn} \qquad (9)$$

In the present treatment, the values of z_n and $\langle E\rangle_n$ required in the calculation have been obtained from F-45 estimated at around T_m. In Table 3, the results of calculations are favorably compared with the experimental values of the constant-volume entropy taken from Paper 1. The uncertainties involved in these experimental values are estimated to be 30−40%.[1]

As mentioned in the preceding section, adoption of the simulation according to eq 6 may lead to suppression of some minor fractions, especially in the case of CBA-10 (see also the Appendix). The effect can be estimated by the expression $\ln(z_n'/z_n)$ (=−0.72 at T_{ni}), where z_n' represents the conformational partition function obtained from F-45 after the simulation. Use of z_n' in eqs 8 and 9 gives rise to an appreciable enhancement in $(\Delta S_{ni})_v$ (=29.4 J mol^{-1} K^{-1}) and a corresponding reduction in $(\Delta S_{cn})_v$ (=49.7 J mol^{-1} K^{-1}). In contrast, the difference between z_n and z_n' was found to be trivial for CBA-9.

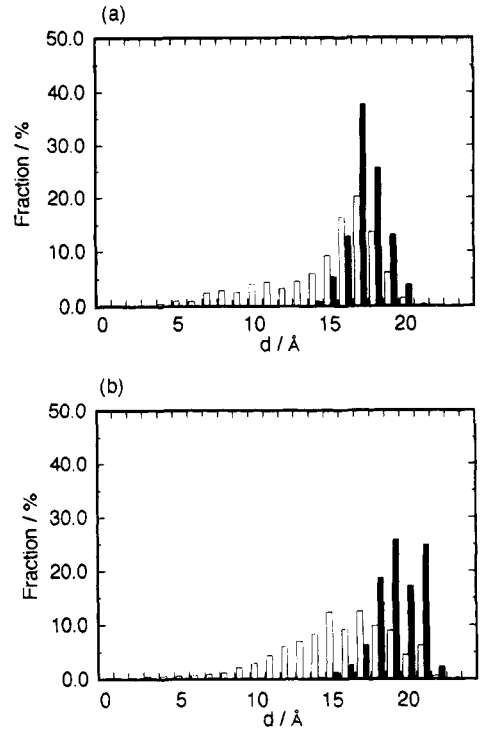

Figure 8. Comparison of the distribution of chain extension d for the isotropic (open) and anisotropic state (filled): (a) CBA-9; (b) CBA-10. Values in the nematic state were taken from F-45 for both CBAs: the distributions are not much affected by the temperature.

5. Discussion

In the aforementioned treatment, the disorientation angle ψ has been adjusted to elucidate a group of conformers which are compatible with the ^{2}H NMR observation. During the iterative calculation, conformer sets which minimize the R factor have been occasionally found outside the ψ_m ranges given above. These sets, however, often involve f_t values considerably lower than those of the isotropic form around certain bonds and thus are discarded for this reason. We also examined conditions other than that ($\psi_1, \psi_2 < \psi_m$) adopted above: e.g., various combinations of the two angles ψ_1 and ψ_2, including $\psi_1 + \psi_2 < 90°$. The simulations according to these schemes yielded more or less similar results. The distribution of the disorientation angle θ between the terminal mesogenic cores provides another measure for the orientational correlation.[13] The analysis indicates that F-45 corresponds to $\theta < 70°$ for CBA-9 and $\theta < 30°$ for CBA-10 in the latter description.

In our previous paper, the magnetic susceptibility data obtained by the SQUID method were shown to be consistent with the results of the ^{2}H NMR/RIS simulation. Following the previous treatment, the anisotropies of the susceptibilities $\Delta\chi_0$ were calculated on the basis of F-45. The $\Delta\chi_0$ values thus derived may be compared with those of the previous estimates (in parentheses) as follows: 1.21 (1.18) (CBA-9) and 1.65 (1.87) (CBA-10) (10^{-8} m^3 kg^{-1} units). The results are essentially unaffected by the modification adopted in this paper.

The bar graphs shown in Figure 8 are the fractional distribution of the distance connecting the centers of the terminal mesogenic cores, which should serve as a measure of the longitudinal extension of molecules. The distributions of the spacer length estimated in the nematic and isotropic states are compared in the diagram. The transition between the two distributions takes place discontinuously around the NI interphase. That is, the transition from the isotropic to the anisotropic phase causes a selection of relatively more elongated species.[25] Eventually in the crystalline state, the most elongated all-trans conformer becomes the only one to survive. Comparison shown in Figure 8 may be useful, although intuitively, in understanding the nature of the nematic state.

In the above treatment, the entropy changes due to the orientation–disorientation of anisotropic molecules at the transitions are not explicitly mentioned. It has been widely accepted that the orientational entropy is one of the most important contributions in the isotropic to the nematic transition of MLCs. In conventional MLC systems, the NI transition takes place when the order parameter of the mesogenic core reaches around 0.3–0.4. The corresponding transition entropies are estimated to be 1.0 J mol^{-1} K^{-1} or less, including some contribution due to the conformational alteration of the tail. In the DLCs under consideration, the order parameters observed at the transition are slightly higher: 0.4–0.6. Although a separate estimation of the orientational entropy is difficult, the contribution involving steric interactions between anisotropic molecules is opposite in sign to the ΔS_{ni}^{conf} calculated above.[13] The discrepancy between the calculated ΔS_{ni}^{conf} and the observed $(\Delta S_{ni})_v$ values may be remedied to some extent by considering such contributions.

As described in Paper 1, the volume dependence of $\gamma = (\partial S/\partial T)_v$ is not known accurately. This leaves some suspicion regarding the possibility of the entropy loss during the compression to achieve constant-volume I → N → C transitions. Since molecules are highly anisotropic in the system, some pressure-induced increase in the trans bond fraction may occur, leading to a decrease in ΔS_{ni}^{conf} as well as ΔS_{cn}^{conf}. This provides another possible explanation for the aforementioned discrepancy between the calculated and observed entropies. In this connection, it may be interesting to note that the order parameters of MLCs such as PAA remain nearly constant at the nematic–isotropic as well as the solid–nematic transition within a certain range of pressure.[26] Similar studies on main chain liquid crystals are not yet available.

In this paper, we have found a reasonable correspondence between the calculated conformational entropies and the observed transition entropies at constant volume for both CBA samples. Our original deduction—"the phase transition entropies $(\Delta S_{tr})_v$ of DLCs may be mostly due to the conformational transformation of the spacer"—has been supported by the results of the present analysis. The important role of the flexible spacer in determining the thermodynamic properties has thus been demonstrated. Further efforts are needed, however, before generalizing the conclusion drawn in this work to other liquid crystals including main chain type PLCs. Studies along this line will be reported elsewhere.

Acknowledgment. The authors are grateful to the Asahi Glass Foundation for financial support of this work.

Appendix. Characterization of Conformer Ensemble F-45 for CBA-10

As a result of an extensive conformer analysis, three major correlation patterns were found in the distribution of F-45:

(1) Odd–even sequences such as t(t,g)t(t,g)t(t,g)t(t,g)t-(t,g)t, where (t,g) indicates a bond which can take either t or $g^{\pm}$ unconditionally. The all-trans configuration may be regarded as a member of the group at one extreme.

(2) Chain sequences characterized by the odd–even trend opposite to that above: i.e., (t,g)t(t,g)t(t,g)t(t,g)t-(t,g)t(t,g), provided that conditions such as ...$g^{+}(t)_h g^{-}$... or ...$g^{-}(t)_h g^{+}$... (with h = odd) are satisfied.

(3) Arrangements consisting of three gauche rotations of the same sign (i.e., g^{+},g^{+},g^{+} or g^{-},g^{-},g^{-}) occurring at proper locations along the chain.

The analysis also indicates that hybrid sequences chosen from the aforementioned categories may also be permitted, provided that the alignment of the terminal mesogenic units remains favorable. In order to investigate the orientational characteristics of the individual conformer groups, RIS simulations were attempted according to the scheme defined by eqs 4–6. The ^2H NMR profiles observed in the vicinity of the NI transition were satisfactorily reproduced by group 2 and moderately well by group 3 (group 3 tends to enhance the order parameter of the molecular axis and thus overestimate D_{HD}). In contrast, however, group 1 alone failed to reproduce the experimental observation. As an inspection of a molecular model should reveal, the disorientation angle of the C–D bonds in terms of $\langle \cos^2 \phi_i \rangle$ fluctuates little with conformation in group 1, leading to a narrower distribution of $\Delta\nu$'s in the calculated spectrum. Nonetheless, the conformations included in this group should play an important role in the nematic ensemble. In fact, the odd–even characteristic inherent to group 1 has been found in the simulation of F-45: see the oscillation indicated by open circles in Figure 7. These results suggest that the conformers satisfying the condition $\psi_1,\psi_2 < 45°$ (cf. Figure 5) are mostly compatible with the nematic order. The conformational analysis indicates that disorientation angles θ defined by the terminal mesogenic units are less than 30° for all conformers involved in F-45.

Shown in Figure 6b are the values of the splitting $\Delta\nu$ directly calculated with conformer ensemble F-45 by using eq 3 (without simulations). The R values are found to be about 10% at both temperatures. The bond conformations derived from F-45 are shown by filled circles in Figure 7b: the trans fraction oscillates moderately in between the two opposite odd–even trends derived from the simulation. Inclusion of conformer group 3 (see above) in F-45 raises the averages of the orientational order parameter of the system. The values of D_{HD} are inevitably overestimated in these calculations.

References and Notes

(1) Abe, A.; Nam, S. Y. *Macromolecules* **1995**, *28*, 90.
(2) Orwoll, R. A.; Sullivan, V. J.; Campbell, G. C. *Mol. Cryst. Liq. Cryst.* **1987**, *149*, 121.
(3) Horn, R. G.; Faber, T. E. *Proc. R. Soc. London* **1979**, *A368*, 199. McColl, J. R.; Shih, C. S. *Phys. Rev. Lett.* **1972**, *29*, 85.
(4) Turturro, A.; Bianchi, U. *J. Chem. Phys.* **1975**, *62*, 1668. Bianchi, U.; Turturro, A. *J. Chem. Phys.* **1976**, *65*, 697.
(5) Béguin, A.; Billard, J.; Bonamy, F.; Buisine, J. M.; Cuvelier, P.; Dubois, J. C.; Le Barny, P. *Mol. Cryst. Liq. Cryst.* **1984**, *115*, 1.

(6) Mandelkern, L. *Crystallization of Polymers*; McGraw-Hill: New York, 1964; Chapter 5.
(7) Kirshenbaum, I. *J. Polym. Sci., Part A* **1965**, *3*, 1869. Tonelli, A. E. *J. Chem. Phys.* **1970**, *52*, 4749. Mark, J. E. *J. Chem. Phys.* **1977**, *67*, 3300. Sundararajan, P. R. *J. Appl. Polym. Sci.* **1978**, *22*, 1391. Abe, A. *Macromolecules* **1980**, *13*, 546.
(8) Starkweather, H. W., Jr.; Boyd, R. H. *J. Phys. Chem.* **1960**, *64*, 410. Smith, R. P. *J. Polym. Sci., Part A-2* **1966**, *4*, 869. Naoki, M.; Tomomatsu, T. *Macromolecules* **1980**, *13*, 322.
(9) Robertson, R. E. *Macromolecules* **1969**, *2*, 250.
(10) Wunderlich, B.; Czornyj, G. *Macromolecules* **1977**, *10*, 906.
(11) Miller, A. A. *Macromolecules* **1979**, *12*, 651.
(12) Bleha, T. *Polymer* **1985**, *26*, 1638.
(13) Abe, A. *Macromolecules* **1984**, *17*, 2280.
(14) Abe, A.; Furuya, H. *Macromolecules* **1989**, *22*, 2982.
(15) Abe, A.; Furuya, H. *Mol. Cryst. Liq. Cryst.* **1988**, *159*, 99. Abe, A.; Furuya, H.; Yoon, D. Y. *Mol. Cryst. Liq. Cryst.* **1988**, *159*, 151.
(16) Inomata, K. Ph.D. Thesis, Tokyo Institute of Technology, 1991.
(17) Abe, A. *Makromol. Chem., Macromol. Symp.* **1992**, *53*, 13.
(18) Furuya, H.; Dries, T.; Fuhrmann, K.; Abe, A.; Ballauff, M.; Fischer, E. W. *Macromolecules* **1990**, *23*, 4122. Furuya, H.; Abe, A.; Fuhrmann, K.; Ballauff, M.; Fischer, E. W. *Macromolecules* **1991**, *24*, 2999.
(19) Abe, A.; Shimizu, R. N.; Furuya, H. *Ordering in Macromolecular Systems*; Teramoto, A., Kobayashi, M., Norisuye, T., Eds.; Springer-Verlag: Berlin, Heidelberg, 1994; p 139.
(20) Blumstein, R. B.; Blumstein, A. *Mol. Cryst. Liq. Cryst.* **1988**, *165*, 361. Volino, F.; Gauthier, M. M.; Giroud-Godquin, A. M.; Blumstein, R. B. *Macromolecules* **1985**, *18*, 2620.
(21) Abe, A.; Furuya, H. *Polym. Bull.* **1988**, *19*, 403. Furuya, H.; Abe, A. *Polym. Bull.* **1988**, *20*, 467.
(22) Kimura, N.; Abe, A. *Polym. Bull.* **1992**, *28*, 81. Abe, A.; Kimua, N.; Nakamura, M. *Makromol. Chem., Theory Simul.* **1992**, *1*, 401.
(23) Malpezzi, L.; Brückner, S.; Galbiati, E.; Luckhurst, G. R. *Mol. Cryst. Liq. Cryst.* **1991**, *195*, 179.
(24) Furuya, H.; Okamoto, S.; Abe, A.; Petekidis, G.; Fytas, G., to be published.
(25) Yoon, D. Y.; Brückner, S. *Macromolecules* **1985**, *18*, 651. Yoon, D. Y.; Brückner, S.; Volksen, W.; Scott, J. C.; Griffin, A. C. *Faraday Discuss. Chem. Soc.* **1985**, *79*, 41. Brückner, S.; Scott, J. C.; Yoon, D. Y.; Griffin, A. *Macromolecules* **1985**, *18*, 2709.
(26) Deloche, B.; Cabane, B.; Jerome, D. *Mol. Cryst. Liq. Cryst.* **1971**, *15*, 197. McColl, J. R. *Phys. Lett.* **1972**, *38A*, 55.

MA941039P